



Seasonal Variability of Sea Surface Salinity in the NW Gulf of Guinea from SMAP Satellite

Ebenezer S. Nyadjro¹ · Bennet A. K. Foli^{2,3} · Kwame A. Agyekum^{2,3} · George Wiafe^{2,3} · Senam Tsei⁴

Received: 30 June 2021 / Revised: 4 October 2021 / Accepted: 25 October 2021 / Published online: 10 November 2021
© The Author(s), under exclusive licence to Springer Nature Switzerland AG 2021

Abstract

The advent of satellite-derived sea surface salinity (SSS) measurements has boosted scientific study in less-sampled ocean regions such as the northwestern Gulf of Guinea (NWGoG). In this study, we examine the seasonal variability of SSS in the NWGoG from the Soil Moisture Active Passive (SMAP) satellite and show that it is well-suited for such regional studies as it is able to reproduce the observed SSS features in the study region. SMAP SSS bias, relative to in-situ data comparisons, reflects the differences between skin layer measurements and bulk surface measurements that have been reported by previous studies. The study results reveal three broad anomalous SSS features: a basin-wide salinification during boreal summer, a basin-wide freshening during winter, and a meridionally oriented frontal system during other seasons. A salt budget estimation suggests that the seasonal SSS variability is dominated by changes in freshwater flux, zonal circulation, and upwelling. Freshwater flux, primarily driven by the seasonally varying Intertropical Convergence Zone, is a dominant contributor to salt budget in all seasons except during fall. Regionally, SSS is most variable off southwestern Nigeria and controlled primarily by westward extensions of the Niger River. Anomalous salty SSS off the coasts of Cote d'Ivoire and Ghana especially during summer are driven mainly by coastal upwelling and horizontal advection.

Keywords Gulf of Guinea · Sea surface salinity · SMAP · Upwelling · Ocean advection · Freshwater flux

1 Introduction

Salinity plays an important role in the global ocean including water mass formation, density and circulation, heat storage, air–sea interactions, and the hydrological cycle [1, 6, 20]. Understanding salinity variability is therefore paramount toward understanding global climate. Salinity changes, especially in the surface ocean, are driven mainly by freshwater flux (i.e., evaporation, precipitation, and river runoff), advection, mixing, and entrainment [16, 47, 49, 54]. In the northwestern Gulf of Guinea (NWGoG: 10°W–5°E, 0°N–7°N;

Fig. 1), the region of focus in this study, the presence and seasonal variability of the Intertropical Convergence Zone (ITCZ) induce significant precipitation and associated river discharges (such as from the Niger, Volta, Tano, and Bandama Rivers; Fig. 2a) which have a substantial influence on sea surface salinity (SSS) variability [15, 22, 58].

Freshwater from precipitation and river discharge modify the vertical stratification of the upper ocean [56]. Ocean stratification, in turn, modulates the availability of subsurface, nutrient-rich waters to the ocean surface which stimulates primary productivity and fish abundance, an important protein need for West Africans [4]. In addition, salinity variability affects the formation of barrier layers (i.e., the difference between the mixed layer depth and isothermal layer depth), which in turn affects air–sea interactions and the West African monsoon [13, 22, 24]. The West African monsoon significantly impacts rainfall occurrence and variability, key factors that control agricultural activities in West Africa [30, 40]. Thus, given the extreme importance of agriculture to the socio-economic lives of West Africans, understanding the variability of salinity in the NWGoG goes beyond oceanographic significance.

✉ Ebenezer S. Nyadjro
esn31@msstate.edu

¹ Northern Gulf Institute, Mississippi State University, Stennis Space Center, MS, USA

² Department of Marine and Fisheries Sciences, University of Ghana, Legon, Ghana

³ Global Monitoring for Environment and Security and Africa, University of Ghana, Legon, Ghana

⁴ School of Ocean Science and Engineering, University of Southern Mississippi, Stennis Space Center, MS, USA

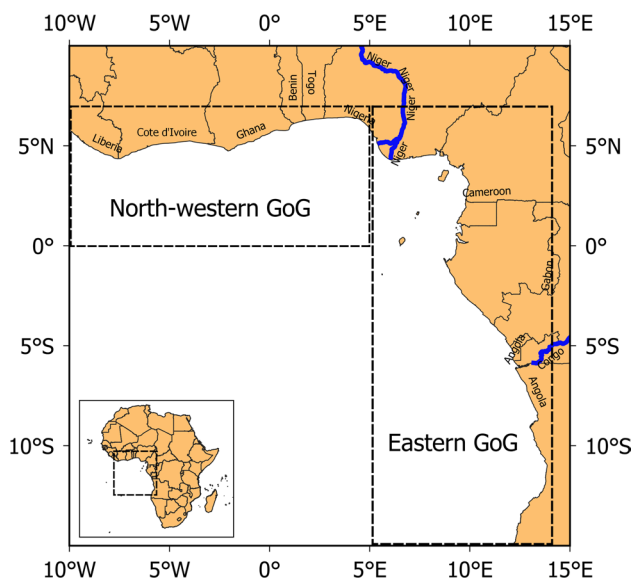
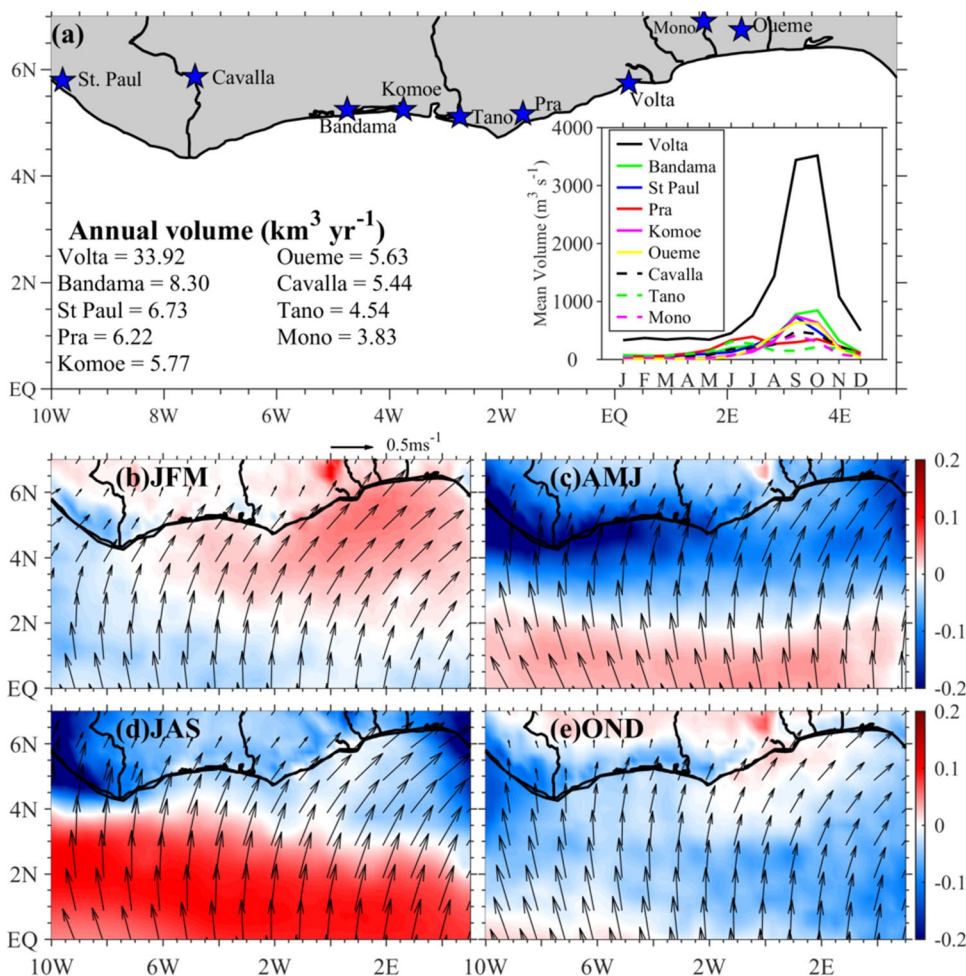


Fig. 1 Map of the Gulf of Guinea highlighting the northwestern Gulf of Guinea study area (10°W–5°E, 0°N–7°N) and the eastern Gulf of Guinea

The wind regime in the Gulf of Guinea (GoG) is dominated by moisture-laden southeasterly winds during boreal summer when the ITCZ lies in its northern position and dry northeasterly winds during boreal winter when the ITCZ retreats southward and precipitation subsides in the subregion [26, 42]. Ocean circulation in the GoG is characterized mainly by the Guinea Current, the equatorial undercurrent (EUC), and the south equatorial current [9, 33]. The eastward flowing Guinea Current is stronger during summer and weaker during winter [2, 8]. A Guinea Undercurrent develops during summer and counterflows in the westward direction underneath the Guinea Current [25]. As the Guinea Current intensifies during summer, it aids upwelling through isothermal displacements resulting from local and remote wind forcing and contributes to salinity variability [3, 33, 38].

Examining salt budget enables the understanding of the relative roles and contributions of the aforementioned physical processes to SSS variability in the NWGoG. Most previous regional studies on SSS (e.g., [5, 14, 34] have focused on the eastern GoG, perhaps due to the strong influence and variability of the Niger River and Congo River on SSS

Fig. 2 (a) Annual mean and seasonal climatology of river (blue star) discharge into the NWGoG. Seasonal mean of evaporation minus precipitation (color shading, $m\ month^{-1}$) and surface winds (vectors, ms^{-1}) during (b) January–March, (c) April–June, (d) July–September, and (e) October–December



variability (Fig. 1). Nevertheless, there is an important contribution from the NWGoG to the GoG SSS variability due primarily to the strong upwelling in the region and the flow of the Guinea Current that circulates mass across the GoG. A study by Camara et al. [12] suggested that the seasonal cycle of mixed layer salinity in the tropical Atlantic Ocean was generally weak due to the strong compensation of the components of the salt budget. [17], however, indicated that freshwater flux was the dominant cause of SSS variability in the GoG during October to February, while horizontal advection and entrainment were the main controlling factors during August to September. Similarly, Dessier and Donguy [21] observed that seasonal SSS variability in the eastern tropical Atlantic Ocean was controlled mainly by ITCZ-influenced precipitation.

Most of the above-mentioned studies used sparsely distributed in-situ data which impacted the understanding of the SSS variability. Satellite measurements of SSS using 1.4 GHz L-band microwave sensors aboard the European Space Agency's Soil Moisture and Ocean Salinity (SMOS; launched November 2009), the US National Aeronautics and Space Administration (NASA)/Argentina Space Agency's Aquarius (June 2011 to June 2015), and the NASA Soil Moisture Active Passive (SMAP; launched January 2015) missions have fostered oceanographic and climate-related studies. Since its launch, SMAP data have been successfully evaluated and used in several oceanographic settings and found to reproduce, and in many instances, better characterize the surface salinity structure (e.g., [27, 31, 45, 48, 57]). Grodsky et al. [29] examined SMAP in the coastal waters of the Gulf of Maine and found the monthly SSS anomalies to be sufficiently accurate and applicable for coastal studies. Hall et al. [32] used SMAP and SMOS in the Arctic and found them to successfully capture sea ice extent and SSS variability, while Hackert et al. [31] demonstrated that including SMAP into the initialization of coupled model forecasts had positive impacts. Despite its quite extensive, successful applications in other seas and ocean basins, to date, and to the best of our knowledge, there has not been any dedicated study aimed at examining SSS variability from SMAP in the NWGoG. In this paper, we evaluate the performance of SMAP SSS in the NWGoG and then use it to understand the seasonal changes in surface salinity and the mechanisms responsible for such changes. The rest of the paper is structured as follows: In "Data and Methods," we introduce the datasets and methods. In "Results and Discussion," we present results of the data consistency evaluation, mean characteristics of SSS, and seasonal variations. We also estimate the SSS budget and examine the main controlling terms. Finally, in "Summary and Conclusion," we provide a summary and conclusions of the study.

2 Data and Methods

2.1 Data

In this study, we used monthly $0.25^\circ \times 0.25^\circ$ gridded Level-3 SSS data obtained from the SMAP v5.0 product produced by the National Aeronautics and Space Administration (NASA) Jet Propulsion Laboratory (JPL; <https://smap.jpl.nasa.gov/data/>) and covers from April 2015 to December 2020. The SMAP satellite measures ocean surface brightness temperature (TB) from which SSS is then retrieved. The satellite has a footprint of ~ 40 m and a global temporal resolution of 3 days, from which the monthly, gridded products are produced. Monthly $0.25^\circ \times 0.25^\circ$ gridded evaporation and precipitation data, available from 1979 to the present, were obtained from the European Centre for Medium-Range Weather Forecasts (ECMWF) Reanalysis v5 (ERA5) dataset. River runoff data was obtained from Dai and Trenberth [18] and contains available monthly river flow rates observed at the farthest downstream station of the respective rivers.

Surface wind data from the v2.0, 6-hourly ocean gap-free $0.25^\circ \times 0.25^\circ$ gridded Remote Sensing Systems' (RSS) Cross-Calibrated Multi-Platform (CCMP) product are used in this study [43]. This product, available from 1988 to the present, is produced by combining cross-calibrated satellite microwave winds and instrument observations using a variational analysis method (VAM). Monthly means were computed from the 6-hourly mean wind fields. We obtained $1^\circ \times 1^\circ$ gridded surface velocity currents from the Ocean Surface Current Analysis Real-Time (OSCAR) dataset [7]. These ocean current data are produced by combining satellite-derived ocean SST, surface heights, and surface winds, using a diagnostic model of ocean currents based on frictional and geostrophic dynamics. OSCAR data represent mean currents in the upper 30 m of the ocean.

Subsurface ocean data were obtained from the Coriolis Ocean Database Reanalysis (CORA v5.2; [11]) $0.5^\circ \times 0.5^\circ$ gridded temperature and salinity product. The CORA product is produced by objective analysis of data from several sources such as Argo floats, sea mammal, conductivity–temperature–depth (CTD), expendable CTDs (XCTD), moorings, and expendable bathythermographs (XBTs).

2.2 Methods

We computed mixed layer depth (MLD) from the CORA dataset using a variable density threshold equivalent to 0.2°C [19]:

$$\Delta\sigma_\theta = \sigma_\theta(T_{10} - 0.2, S_{10}, P_0) - \sigma_\theta(T_{10}, S_{10}, P_0) \quad (1)$$

where $\Delta\sigma_\theta$ is the change in potential density between a reference depth (here taken as the 10 dbar) and the base of

the mixed layer. T_{10} and S_{10} are, respectively, temperature and salinity at 10 dbar, and P_0 is sea surface pressure. The isothermal layer depth (ILD) is computed as the depth at which the subsurface temperature decreases by 0.2°C relative to the temperature at the reference depth of 10 dbar. Subsequently, the barrier layer thickness, $\text{BLT} = \text{ILD} - \text{MLD}$.

We estimated SMAP salt budget as in Bingham et al. [6], Nyadjro and Subrahmanyam [50], and Sommer et al. [54]:

$$\frac{\partial S}{\partial t} = S \frac{(E - P - R)}{h} - u \frac{\partial S}{\partial x} - v \frac{\partial S}{\partial y} - w \frac{\partial S}{\partial z} + D \quad (2)$$

where S is the SMAP SSS, E is evaporation, P is precipitation, R is river runoff, h is the MLD, u is zonal current velocity, v is meridional current velocity, and w is vertical current velocity. w is obtained by combining the Ekman upwelling (w_e ; computed from CCMP winds product) and vertical motion of the mixed layer (i.e., vertical entrainment rate), $w = w_e + \partial h / \partial t$, where $w_e = \text{curl}(\tau) / \rho f$, τ is wind stress, f is Coriolis parameter, and ρ is the surface density computed from the CORA data. D is the residual from the salt budget computation and represents computational errors and physical processes (e.g., lateral and vertical mixing processes) that cannot be estimated directly from the datasets used for the computations. The vertical salinity gradient was obtained from the CORA data as the difference between the SSS and salinity 10 m below the MLD [54]. The terms in Eq. (2) from left to right are the SSS tendency, sea surface freshwater forcing, zonal salt advection, meridional salt advection, surface–subsurface interaction, and residuals.

We compute seasonal anomalies as the difference between monthly climatologies and the data mean, where means are computed over the period covering the SMAP data for this study (i.e., April 2015–December 2020). For the computation of salt budget terms, all data were linearly interpolated to the SMAP grid.

3 Results and Discussion

3.1 Assessment of SMAP SSS

We evaluate the performance of SMAP SSS in the NWGoG by comparing it to the CORA SSS dataset. We use January and August SSS climatologies to respectively represent SSS during the boreal winter and summer seasons (Fig. 3). Generally, the SSS representation is stronger in SMAP relative to the CORA dataset. In particular, higher SSS occurs off the coastal upwelling areas of Cote d’Ivoire and Ghana in SMAP, with the SSS difference being larger during summer than winter (Fig. 3). Strong upwelling at these locations during summer brings cooler, saltier subsurface waters to the surface ocean [3, 60]. SMAP resolves this higher salinity better than CORA. The northeastern-most section of the study area, off the coasts of Togo to southwestern Nigeria, is dominated by freshwater from the northwestern arm of the Niger River. At this location, SSS is much fresher in SMAP than in CORA, with the SSS difference being larger during winter than summer (Fig. 3c, f).

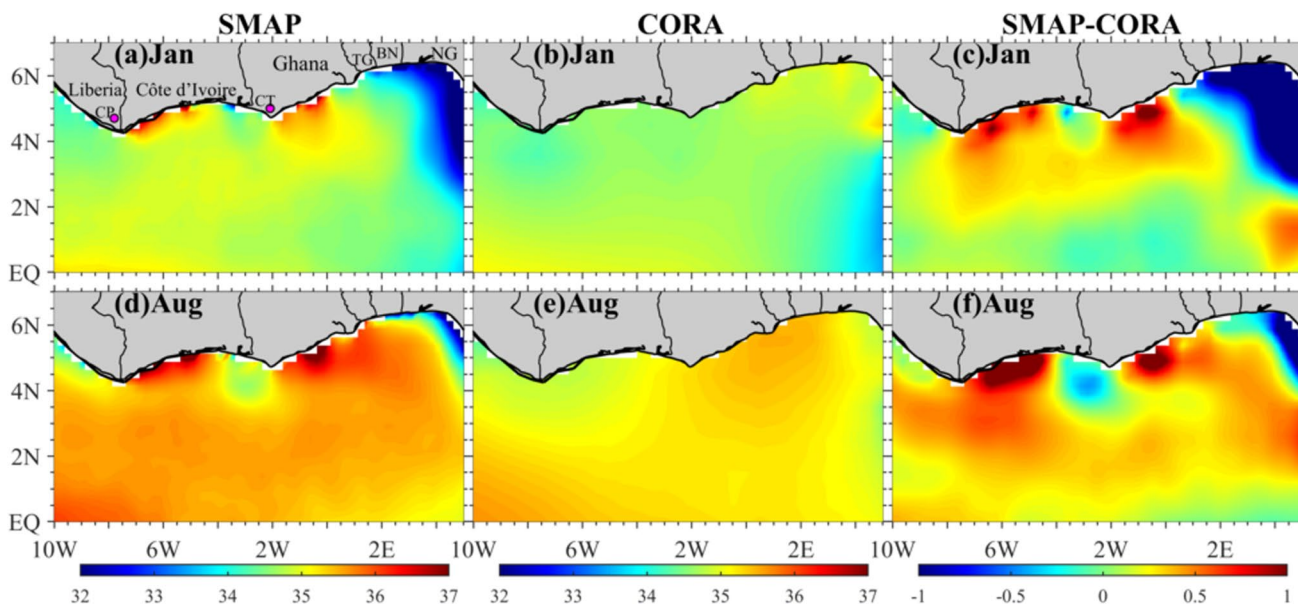


Fig. 3 Comparison of SMAP (left column) and CORA SSS (PSU) (middle column) during January (upper row) and August (lower row). The right column represents SMAP minus CORA SSS

SMAP measures SSS at the skin layer, typically 1–3 cm [10], while the in-situ input data (mainly CTDs and Argo profiles) ingested for the CORA product measure “surface salinity” at ~5–10 m (i.e., bulk surface measurement; [1]. The SSS differences between these two products can thus be relatively large in strong freshwater-controlled areas due to strong vertical stratification [10, 39, 53]. In well-mixed areas, skin-layer SSS is approximately similar to a bulk surface (e.g., at 5 m) SSS, while in freshwater (evaporation)-dominated areas, skin-layer SSS is significantly fresher (saltier) than bulk surface SSS [10]. In addition, it should be noted that the CORA dataset is produced by highly smoothing point-wise, sparsely distributed in-situ measurements. For example, Argo floats typically cover a $3^{\circ} \times 3^{\circ}$ area [35, 51]. Such spatial smoothing also generates a mismatch between satellite measurements and in-situ observations especially in areas where the SSS has significant temporal and spatial variability [10, 34]. This partly explains the spatial bias between SMAP and CORA in the highly variable SSS coastal areas of the NWGoG (Fig. 3). The seasonal differences in the fresh bias could be attributed to the increased stratification during winter that arises from the larger fall river discharge (Fig. 2) and weaker winds (Fig. 2e) which do not induce strong mixing of the upper water column [10, 23]. From the aforementioned, skin-layer SSS from satellites such as SMAP exhibits greater seasonal variability especially in tropical areas of high stratification and horizontal heterogeneity and is often considered to be a true reflection of SSS than bulk surface salinity measurements [46, 55].

The most recent SMAP satellite data, which is used in this study, shows the availability of SSS data closer to the coast (i.e., within 30–40 km from land) than from earlier satellite-based SSS measurements from SMOS and SMAP (e.g., [37, 41, 44, 50, 59]. SSS data, within reasonable proximity to the coast, is critical for our study area as significant coastal upwelling occurs along the NWGoG coast which plays an important role in the SSS variability and dynamics, as we demonstrate later. The improvements in coastal SSS retrieval have been possible due to reductions in man-made radio-frequency interference (RFI) which infringes on the 1.4-GHz L-band frequency reserved for scientific studies [45]. In addition, recent improvements in SSS retrieval algorithms have led to better corrections of land contamination, thereby enhancing SMAP’s reliability for coastal area studies [28, 29, 45].

3.2 Annual Mean

The long-term mean (i.e., computed for April 2015–December 2020) SSS shows relatively high surface salinity waters along the coasts of Ghana and Cote d’Ivoire with relatively fresher water near their boundary (Fig. 4a) that is largely influenced by discharge from the Tano River in the

southwestern-most part of Ghana and the Komoé River in southeastern Cote d’Ivoire (Fig. 2a). The freshest surface waters (< 32 PSU) occur in the northeastern-most part of the study region, largely influenced by the northwestward extension of the Niger River plume (Fig. 4a). This is also the region where SSS undergoes the most seasonal variability (Fig. 4b). On an annual scale, the NWGoG is precipitation-dominated, as annual mean precipitation (Fig. 4e) exceeds annual mean evaporation (Fig. 4c). The weak seasonal variability of evaporation (Fig. 4d) is due to the location of the study area in the equatorial region which ensures nearly year-round insolation. The seasonal variability of precipitation (Fig. 4f) is largely due to the presence and seasonal displacement of the rain-laden ITCZ in the study area [26, 30, 42]. While annual mean precipitation is largest (> 0.2 m month⁻¹, Fig. 4e) and also most seasonally variable (Fig. 4f) in Liberia in the northwestern section of the study region, SSS here is not as low as in the northeastern section of the study region (Fig. 4a). SSS seasonal variability is weak in the open ocean (Fig. 4b) as SSS controlling factors are relatively weak in this region (Fig. 4).

3.3 SSS Seasonal Cycle

The seasonal cycle of box-averaged SSS time series in the NWGoG is presented in Fig. 5. The boxes for the averaging (i.e., Area-A, Area-B, Area-C, and Area-D; Fig. 4b) are chosen based on the aforementioned regional characteristics of SSS. Shaded areas show the monthly standard deviations of the SSS seasonal anomalies (Fig. 5a). SSS in the NWGoG predominantly exhibit an annual cycle with maxima during summer and minima during winter. At each location, the strongest standard deviation of seasonal anomalies occurs during the winter months. In all areas except in the open ocean (i.e., Area-D), the highest SSS is recorded during the summer and lowest during the later fall and winter. The lowering of SSS after summer coincides with the period when river discharge is at the highest in the NWGoG (Fig. 2a).

The time series plot shows the northeastern region (i.e., Area-C in Fig. 5b) to be the most variable area, with stronger SSS variability during winter than summer. The lowest SSS (~ 31.7 PSU) occurs during November after which the SSS increases and peaks during the summer, with the highest SSS (~ 35.1 PSU) occurring during August. On the contrary, the least variable region is the open ocean, away from the coastal area, where a relatively high SSS is recorded during summer through the fall. At this location, the lowest SSS (~ 34.6 PSU) occurs during May while the highest SSS (~ 35.6 PSU) occurs during September. This is possibly influenced by the cyclonic flow that develops during summer and fall and distributes high SSS from the coastal areas (Fig. 6h–j). SSS off the coasts of Cote d’Ivoire (i.e., Area-A) and Ghana (i.e., Area-B) are mostly saltier in many months

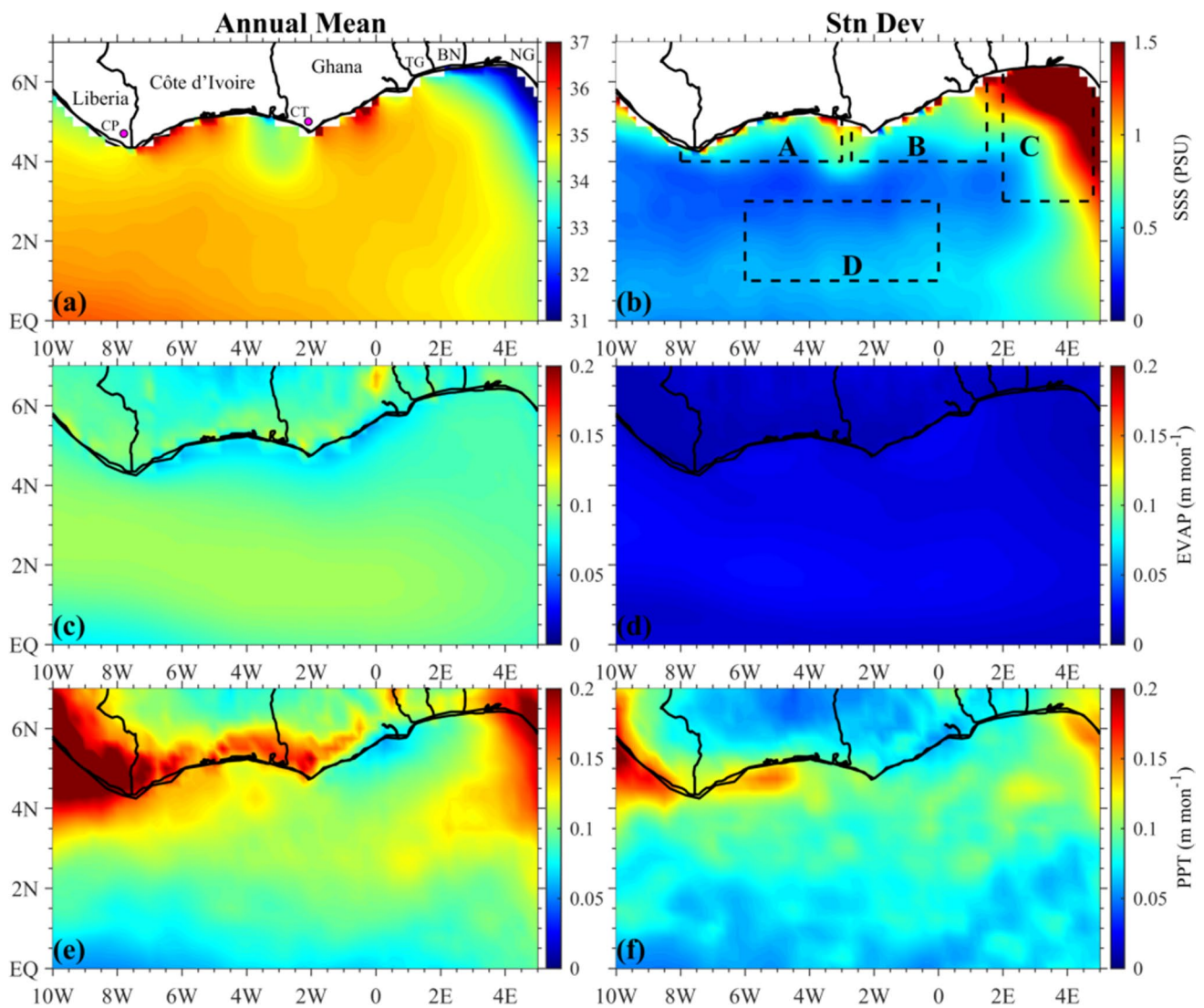


Fig. 4 Annual mean (left column) and seasonal standard deviation (right column) of SSS (PSU) (top row), evaporation (m month^{-1}) (middle row), and precipitation (m month^{-1}) (bottom row). Regional delineations in (b) are used for box-averaging

than at the other locations and tend to track each other quite closely (Fig. 5a). Indeed, the mean SSS at these two locations are statistically indistinguishable at the 95% confidence level ($p=0.299$). Along the coast of Cote d'Ivoire, the lowest SSS (34.2 PSU) occurs during October, while the highest SSS (35.6 PSU) occurs during August. Similarly, along the coast of Ghana, the lowest SSS (34.1 PSU) occurs during November, while the highest SSS (35.8 PSU) occurs during August. These SMAP-observed SSS variabilities are consistent with previous studies (e.g., [15, 16, 22]).

Year-to-year differences in the regional SSS are noted in the study area, especially in the northeastern section of the study area. For example, during the winter of 2015, a regional high SSS of ~ 33 PSU was recorded in the northeastern section of the study area, which dropped to ~ 31 PSU during the winter of 2018 (Fig. 5b). This variability could

be attributed to the significant interannual variability in the Niger River discharge [5, 22].

The spatio-temporal variations of sea surface salinity seasonal anomalies (SSSA) and surface current seasonal anomalies in the NWGoG are presented in Fig. 6. Three broad seasonal SSSA features can be delineated: a basin-wide salinification during summer, a basin-wide freshening during winter, and a meridionally oriented frontal system during other seasons. Notable SSSA fronts occur during October–November (Fig. 6j, k) and February–April (Fig. 6b–d). These may induce air–sea interactions and cause precipitation. Indeed, the fronts during February–April precede the major rainy season across the NWGoG (Fig. 6c; [26, 42]). The SSSA frontal structure during February–April is composed of anomalous high SSS poleward of 3.5°N and anomalous low SSS equatorward of 3.5°N . This is a reverse of the

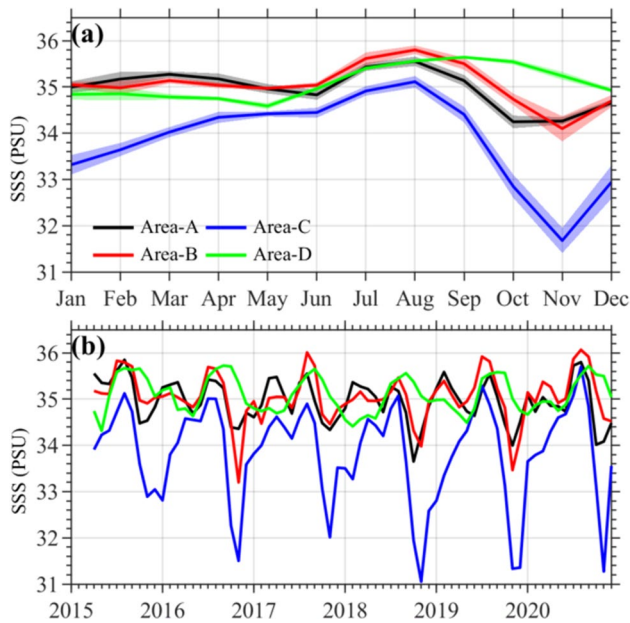


Fig. 5 (a) Seasonal cycle and (b) yearly variations of SSS (PSU) box-averaged for the regions shown in Fig. 4b. Shadings in (a) show seasonal standard deviations

spatial structure of the SSS fronts that formed during October–November, after the major upwelling season (Fig. 6j, k). Weaker coastal salinification during winter–spring can be linked to the secondary upwelling season [16]. Following

the spring and early summer rainfall (Fig. 2c), river runoff increases during summer and peaks during fall (Fig. 2a). The precipitation and summer runoff do not freshen the SSS as net freshwater flux is overwhelmed by high salinity waters from the subsurface that results from the strong summer upwelling. After the summer upwelling, when the river runoff reaches its peak, it aids the freshening of the surface waters.

3.4 Subsurface Influence

The subsurface influence on the surface ocean is typically controlled by wind forcing, mixed layer thickness, ocean stratification, and upwelling source depth [36, 52]. Plots of box-averaged salinity and temperature seasonal anomalies in the upper 100 m of the subregions in Fig. 4b show strong seasonal variability of salinity and temperature (Fig. 7), driven mostly by changes in the thermocline depth and upwelling. The upper 40 m in the subregions are characterized by anomalous salty waters during summer. In the spring, there is a weaker anomalous salinification in the upper 20 m in the coastal subregions of the study area (Fig. 7a–c). The rest of the seasons are characterized by anomalous freshwater. Likewise, anomalously cooler temperatures predominantly occupy the water column during summer, while anomalously warmer temperatures occur during the rest of the seasons (Fig. 7b).

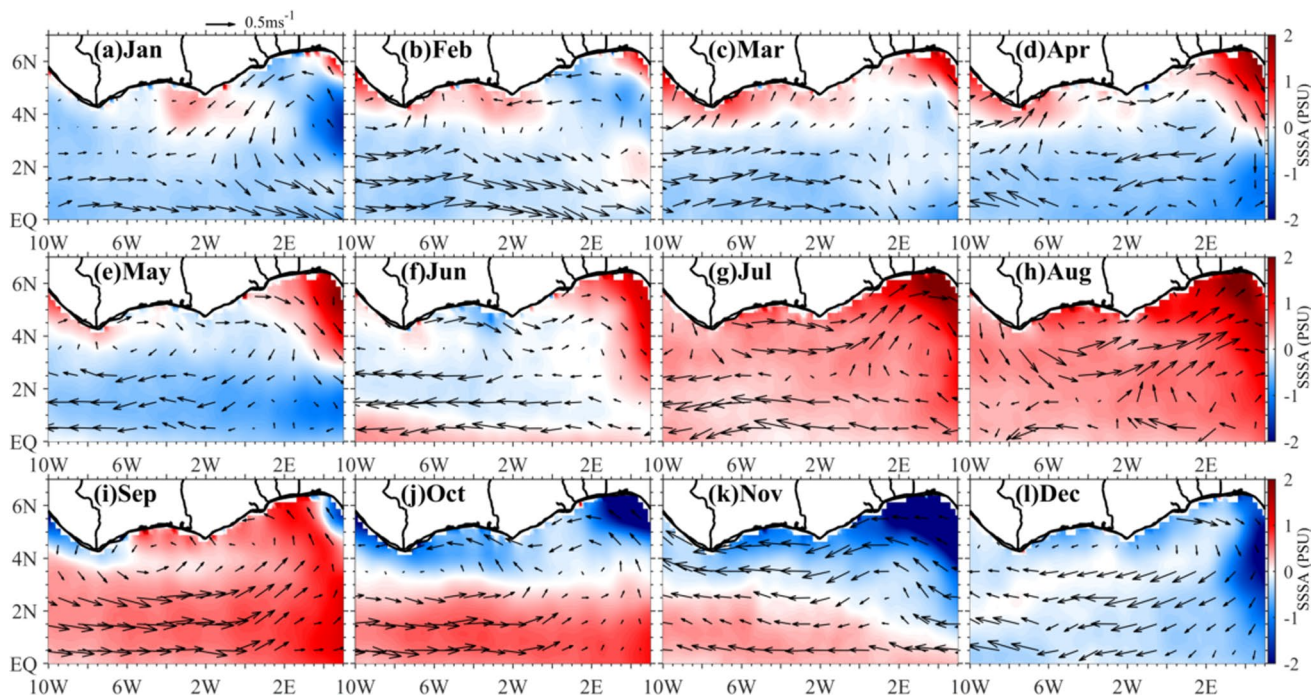


Fig. 6 Seasonal anomalies of SSS (color shading, PSU) and surface currents (vectors, ms^{-1})

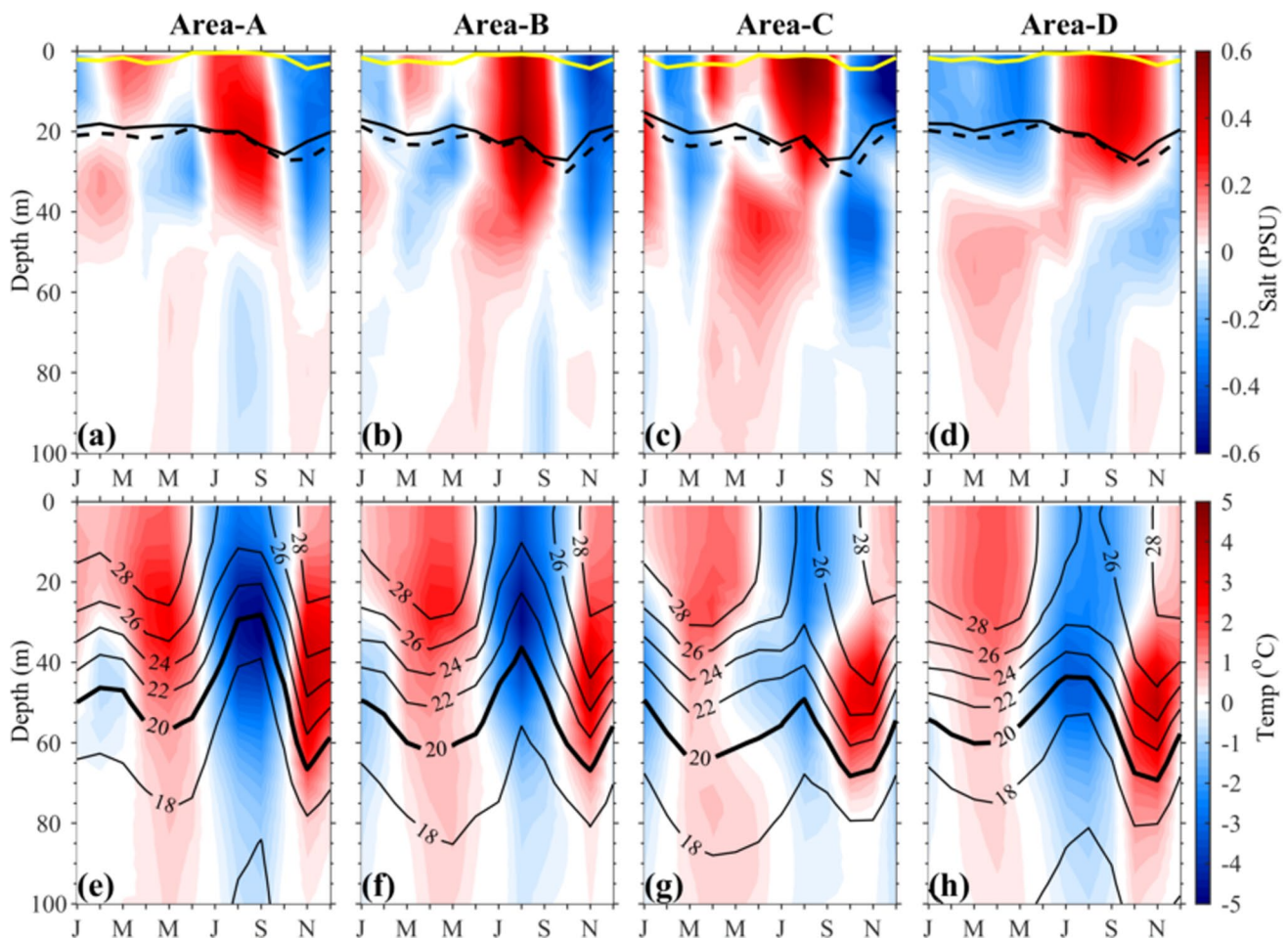


Fig. 7 Time-depth sections of CORA seasonal anomalies of salinity (color shading, PSU) (top row), and temperature (color shading, °C) (bottom row), box-averaged for the regions shown in Fig. 4b. Solid black lines, dashed black lines, and yellow lines in (a) respectively

show the mixed layer depth (MLD, m), isothermal layer depth (ILD, m), and the barrier layer thickness (BLT=ILD–MLD). Solid black lines in (b) show isotherms (°C, CI=4°C). See Fig. 4b for locations of boxes

The summer cooling and salinification result from shoaling of the thermocline, with stronger shoaling and cooler waters off Cote d’Ivoire (Fig. 7e) and Ghana (Fig. 7f) than other areas. This upwelling, which also lifts the ILD and breaks any existing barrier layers, enables the entrainment of subsurface saltier waters into the surface ocean (Fig. 7). Outside of the summer upwelling season, a deepening of the thermocline is associated with anomalous warming in the water column. In addition, the ILD is deeper than the MLD which creates a barrier layer and restrains the advection of subsurface waters to the surface ocean. Generally, the barrier layer in the study area is strongest during spring and winter (Fig. 7), consistent with previous results by Dossa et al. [22]. The spring barrier layer possibly forms from precipitation which is at its peak during this season in the NWGoG (Fig. 2c). The winter barrier layer, on the other hand, possibly forms from the peak fall river runoff (Fig. 2a,[22]).

Although the thermocline depth is shallowest off the coast of Cote d’Ivoire (Fig. 7), Ekman upwelling is persistent and strongest in the northeastern half of the study area, from Ghana to southwestern Nigeria (Fig. 8). Peak upwelling occurs during the major upwelling season in summer and typically exceeds $1 \times 10^{-5} \text{ ms}^{-1}$, while during the minor upwelling season in winter, the upwelling could reach $0.5 \times 10^{-5} \text{ ms}^{-1}$ (Fig. 8). Possible explanations for the observed regional differences in upwelling include the fact that the winds are more aligned to the coast and thus more upwelling-favorable in the northeastern half of the study area than in the northwestern half (Fig. 2). Further in the northwest, especially along the Liberian coast, the winds are nearly perpendicular to the coastline (i.e., unfavorable for upwelling; Fig. 2) and explains the strong downwelling during summer and weak upwelling during other seasons in that region. It should be noted that remote contributions to thermocline displacements and upwelling, which could be

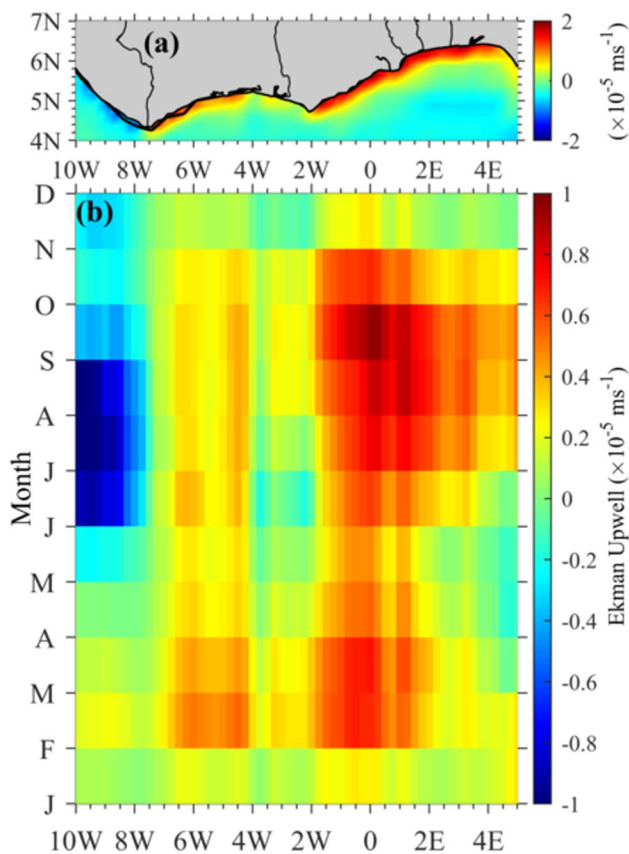


Fig. 8 (a) Annual mean and (b) seasonal cycle of Ekman pumping (ms^{-1}) averaged in the NWGoG coastal area

important in the NWGoG [38, 60], have not been included in these. Thus, the subsurface contributions could be underestimated in this study.

3.5 Salt Budget Estimation

Figure 9 presents seasonal composites of contributions of the terms in Eq. (2) to SSS changes in the NWGoG. The SSS budget is driven mainly by freshwater flux, zonal advection, and upwelling, with the relative contributions of these physical mechanisms varying in both time and space. Generally, there is a near basin-wide tendency for salinification during April–June (~ 0.5 PSU/month) and a tendency for freshening during October–December (~ -0.5 PSU/month). On the other hand, there is a tendency for salinification in the coastal areas (~ 0.5 PSU/month) and freshening in the open ocean (~ -0.3 PSU/month) during January–March. This spatial pattern reverses during July–September with a tendency for freshening observed in the coastal areas (~ -0.4 PSU/month) and salinification in the open ocean (~ 0.4 PSU/month; Fig. 9). Noteworthy is that the above-mentioned SSS tendencies align well in sign with the net freshwater flux distribution except during April–June when

there is negative freshwater flux north of 2°N (Fig. 9f), yet a dominant tendency for salinification occurs (Fig. 9b). The alignment in sign suggests a relatively dominant contribution of the freshwater flux term to the salinity tendency in the NWGoG. While April–June marks the period of peak precipitation in the NWGoG (Fig. 2c), it only leads to freshening along the coasts of Liberia and Cote d’Ivoire during this season (Fig. 9b).

Throughout the year, zonal advection increases SSS in the northwestern part of the study area, especially off the coast of Cote d’Ivoire, and it is the main driver of the salinity tendency in that area during January–March (Fig. 9a). This physical mechanism is also important for salinification in the southeastern part of the study region during January–September (Fig. 9i–k). In the northeastern part of the study region, zonal advection contributes to freshening during all the seasons except during April–June, when it leads to salinification. Meridional advection, on the other hand, dominantly causes freshening in the coastal waters from Liberia to Ghana during January–September. During winter, however, meridional advection leads to strong salinification in the study area except off the Liberian coast where it causes freshening (Fig. 9p).

The impact of the subsurface term on the SSS budget is dominant mainly in the coastal waters and weak in the open ocean (Fig. 9, lower panel). It presents three main categories of contributions to the SSS changes: freshening in the northwestern part of the study area, salinification in the northeastern part of the study area during January to September, and salinification along the coast during October to December. Indeed, the salinification effects from the meridional advection (Fig. 9p) and subsurface (Fig. 9t) terms overwhelm the freshening effects from the surface flux (Fig. 9h) and zonal advection (Fig. 9l) terms and cause the positive salinity tendency off southwestern Nigeria during the winter (Fig. 9d). As previously mentioned, local Ekman upwelling alone does not account for all the upwelling that occurs in the region [38, 60]. Remote contributions from Rossby waves as well as the EUC advecting waters from the western Atlantic Ocean toward the NWGoG could be important [2, 25].

4 Summary and Conclusion

There have been limited studies on salinity variability in the NWGoG due to the paucity of in-situ observations. Since its launch, the scientific value of SMAP has increased and enabled the examination of the SSS seasonal variability in the NWGoG. Assessment of SMAP in the study region shows it can reproduce the observed features of SSS distribution in time and space. Notably, the dominant freshwaters off the coast of southwestern Nigeria and the high saline waters off the strong upwelling coastal waters off the coasts of Cote

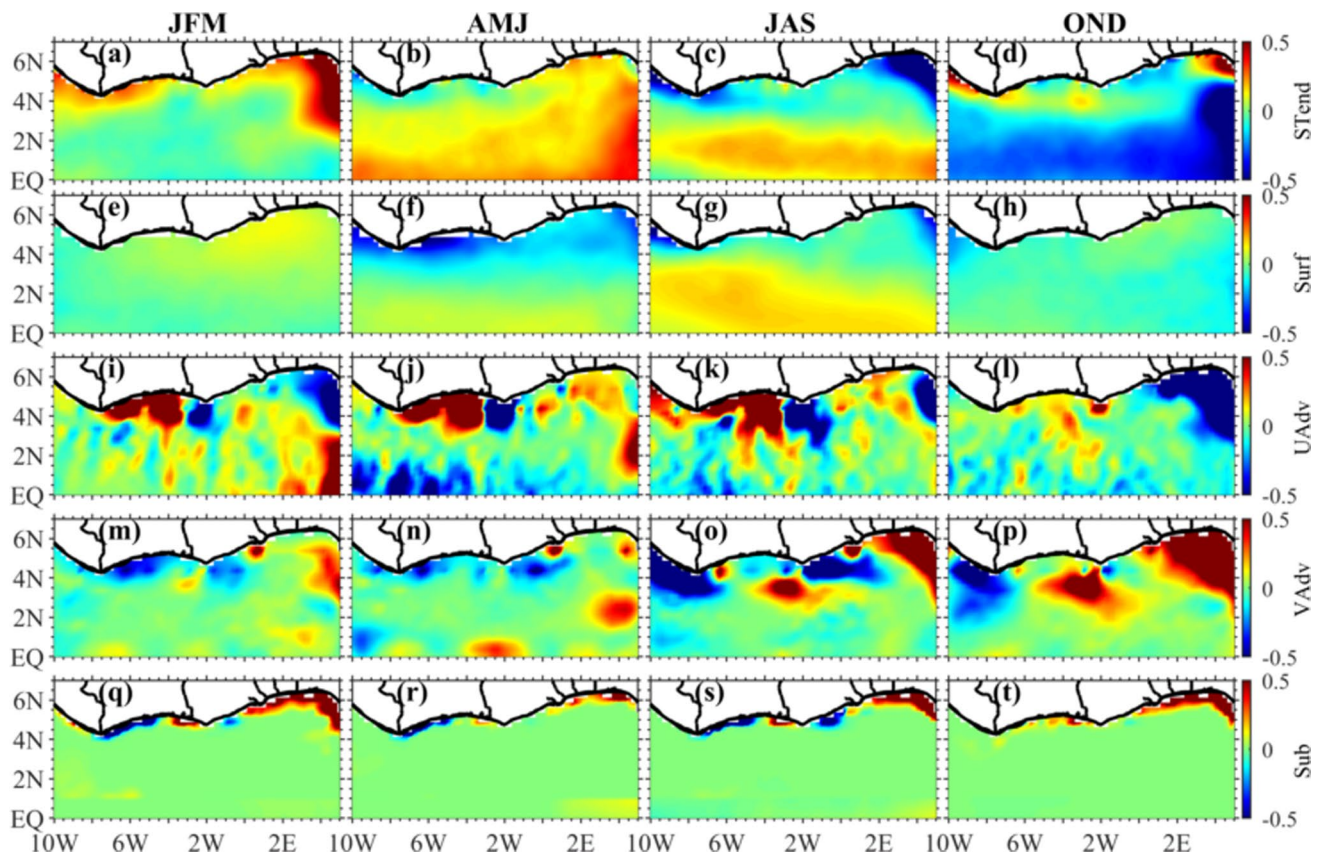


Fig. 9 Tri-monthly composites of salt budget terms (PSU month^{-1}) for salinity tendency (row 1), surface freshwater flux (row 2), zonal advection (UADV) (row 3), meridional advection (VADV) (row 4), and subsurface influence (row 5) during January–March (column 1),

April–June (column 2), July–September (column 3), and October–December (column 4). See Eq. (2) for the definition of salt budget terms

d'Ivoire and Ghana are well represented in SMAP. We found a significant, seasonally varying difference between SMAP and CORA dataset, with SMAP being saltier in high salinity regions and fresher in low salinity regions. These biases most likely arise from the depths at which surface salinity is measured with SMAP measuring the skin-layer SSS and CORA measuring bulk surface salinity.

Our results show SSS in the NWGoG to largely display an annual cycle with maxima in the summer and minima in the winter, mostly driven by ITCZ-influenced precipitation. To better understand regional SSS differences, we computed box averages with results showing that except in the open ocean, the highest regional SSS was recorded during summer and lowest during winter. These differences and variability were supported by changes in the thermocline depth and associated upwelling which brought anomalous salty waters to the surface ocean, especially in the coastal waters. Furthermore, salt budget estimation suggests that horizontal advection contributed to SSS variability in the NWGoG. At the beginning of the year, the contribution from zonal advection overwhelms the freshening impact from

meridional advection and subsurface processes and causes salinification in the northwestern part of the study area. On the other hand, zonal advection contributes to freshening in most seasons in the northeastern part of the study region.

While SMAP improves our ability to understand the SSS variability in the NWGoG, the empirical approach to salt budget estimation as done in this study does not allow us to examine all the possible physical mechanisms that drive SSS changes such as diffusion and remote contribution to upwelling. A complete numerical simulation with SMAP assimilation will further advance our understanding of SSS variability in the NWGoG.

Acknowledgements The authors acknowledge the freely available data obtained from the NASA Jet Propulsion Laboratory, Remote Sensing Systems, and the European Union's Copernicus Marine Service. We thank the anonymous reviewers whose comments helped improve the manuscript.

Data availability SMAP SSS data are available at <https://smap.jpl.nasa.gov/data/>. CCMP Version-2.0 vector wind analyses are produced by Remote Sensing Systems. Data are available at <http://www.remss.com/>

[measurements/ccmp/](#). CORA and ERA5 data are obtained from Copernicus Marine Service, https://resources.marine.copernicus.eu/?option=com_csw&task=results. OSCAR data were obtained from https://podaac-tools.jpl.nasa.gov/drive/files/allData/oscar/L4/oscar_1_deg.

Code Availability None.

Declarations

Conflict of Interest/Competing Interests Authors declare no financial and competing interests.

References

- Anderson JE, Riser SC (2014) Near-surface variability of temperature and salinity in the near-tropical ocean: observations from profiling floats. *J Geophys Res Oceans* 119:7433–7448
- Arhan M, Treguier A, Bourles B, Michel S (2006) Diagnosing the annual cycle of the Equatorial Undercurrent in the Atlantic Ocean from a general circulation model. *J Phys Oceanogr* 36(8):1502–1522
- Bakun A (1978) Guinea current upwelling. *Nature* 271:147–150
- Belhabib D, Rashid Sumaila U, Le Billon P (2019) The fisheries of Africa: exploitation, policy, and maritime security trends. *Mar Policy* 101:80–92
- Berger H, Treguier AM, Perenne N, Talandier C (2014) Dynamical contribution to sea surface salinity variations in the eastern Gulf of Guinea based on numerical modelling. *Clim Dyn* 43:3105–3122
- Bingham FM, Foltz GR, McPhaden MJ (2010) Seasonal cycles of surface layer salinity in the Pacific Ocean. *Ocean Sci* 6:775–787. <https://doi.org/10.5194/os-6-775-2010>
- Bonjean F, Lagerloef GSE (2002) Diagnostic model and analysis of the surface currents in the Tropical Pacific Ocean. *J Phys Oceanogr* 32(10):2938–2954
- Bourlès B, D'Orgeville M, Eldin G, Gouriou Y, Chuchla R, Penhoat YD, Arnault S (2002) On the evolution of the thermocline and subthermocline eastward currents in the Equatorial Atlantic. *Geophys Res Lett* 29(16):1785. <https://doi.org/10.1029/2002GL015098>
- Bourlès B, Molinari RL, Johns E, Wilson WD, Leaman KD (1999) Upper layer currents in the western tropical Atlantic (1989–1991). *J Geophys Res* 104(C1):1361–1375
- Boutin J, Chao Y, Asher WE, Delcroix T, Drucker R, Drushka K, Kolodziejczyk N, Lee T, Reul N, Reverdin G et al (2016) Satellite and in situ salinity: understanding near-surface stratification and subfootprint variability. *Bull Amer Meteor Soc* 97:1391–1407
- Cabanes C, and Coauthors (2013) The CORA dataset: Validation and diagnostics of in-situ ocean temperature and salinity measurements. *Ocean Sci* 9: 1–18
- Camara I, Kolodziejczyk N, Mignot J, Lazar A, Gaye AT (2015) On the seasonal variations of salinity of the tropical Atlantic mixed layer. *J Geophys Res Oceans* 120:4441–4462
- Caniaux G, Giordani H, Redelsperger JL, Guichard F, Key E, Wade M (2011) Coupling between the Atlantic cold tongue and the West African monsoon in boreal spring and summer. *J Geophys Res Oceans*. <https://doi.org/10.1029/2010JC006570>
- Chao Y, Farrara JD, Schumann G, Andreadis KM, Moller D (2015) Sea surface salinity variability in response to the Congo River discharge. *Cont Shelf Res* 99:35–45
- Da-Allada CY, Alory G, Penhoat YD, Kestenare E, Durand F, Hounkonnou N (2013) Seasonal mixed-layer salinity balance in the tropical Atlantic Ocean: mean state and seasonal cycle. *J Geophys Res Oceans* 118(1). <https://doi.org/10.1029/2012JC008357>
- Da-Allada CY, du Penhoat Y, Jouanno J, Alory G, Hounkonnou N (2014) Modeled mixed-layer salinity balance in the Gulf of Guinea: seasonal and interannual variability. *Ocean Dyn* 64(12):1783–1802
- Da-Allada CY, Gaillard F, Kolodziejczyk N (2015) Mixed-layer salinity budget in the tropical Indian Ocean: seasonal cycle based only on observations. *Ocean Dyn* 65:845–857. <https://doi.org/10.1007/s10236-015-0837-7>
- Dai A, Trenberth KE (2002) Estimates of freshwater discharge from continents: latitudinal and seasonal variations. *J Hydrometeorol* 3(6):660–687
- de Boyer MC, Madec G, Fischer AS, Lazar A, Iudicone D (2004) Mixed layer depth over the global ocean: an examination of profile data and a profile-based climatology. *J Geophys Res* 109:C12003. <https://doi.org/10.1029/2004JC002378>
- Delcroix T, Henin C (1991) Seasonal and Interannual variations of the sea surface salinity in the tropical Pacific Ocean. *J Geophys Res* 96:22135–22150
- Dessier A, Donguy JR (1994) The sea surface salinity in the tropical Atlantic between 10°S and 30°N: seasonal and interannual variations (1977–1989). *Deep Sea Res. Part I* 41:81–100
- Dossa A, Da-Allada C, Herbert G, Bourlès B (2019) Seasonal cycle of the salinity barrier layer revealed in the northeastern Gulf of Guinea. *Afr J Mar Sci* 41(2):163–175
- Drushka K, Asher WE, Ward B, Walesby K (2016) Understanding the formation and evolution of rain-formed fresh lenses at the ocean surface. *J Geophys Res Oceans* 121:2673–2689
- Foltz GR, McPhaden MJ (2009) Impact of barrier layer thickness on SST in the central tropical North Atlantic. *J Clim* 22(2):285–299
- Giarolla E, Nobre P, Malagutti M, Pezzi L (2005) The Atlantic Equatorial Undercurrent: PIRATA observations and simulations with GFDL Modular Ocean model at CPTEC. *Geophys Res Lett*, 32(10): L10 617. <http://www.agu.org/journals/ABS/2005/2004GL022206.shtml>.
- Grist JP, Nicholson SE (2001) A study of the dynamics factors influencing the rainfall variability in the West African Sahel. *J of Clim* 14:1337–1359
- Grodsky SA, Reul N, Bentamy A, Vandemark D, Guimbarde S (2019) Eastern Mediterranean salinification observed in satellite salinity from SMAP mission. *J Mar Sys* 198:103190. <https://doi.org/10.1016/j.jmarsys.2019.103190>
- Grodsky SA, Vandemark D, Feng H (2018) Assessing coastal SMAP surface salinity accuracy and its application to monitoring Gulf of Maine circulation dynamics. *Remote Sens* 10(8):1232. <https://doi.org/10.3390/rs10081232>
- Grodsky SA, Vandemark D, Feng H, Levin J (2018) Satellite detection of an unusual intrusion of salty slope water into a marginal sea: using SMAP to monitor Gulf of Maine inflows. *Remote Sens Environ* 217:550–561
- Gu G, Adler RF (2004) Seasonal evolution and variability associated with the west African monsoon system. *J Clim* 17:3364–3377
- Hackert EC, Kovach RM, Busalacchi AJ, Ballabrera-Poy J (2019) Impact of Aquarius and SMAP satellite sea surface salinity observations on coupled El Niño/Southern Oscillation forecasts. *J Geophys Res* 124. <https://doi.org/10.1029/2019JC015130>
- Hall SB, Subrahmanyam B, Nyadjro ES, Samuelsen A (2021) Surface freshwater fluxes in the Arctic and Subarctic Seas during contrasting years of high and low summer sea ice extent. *Remote Sens* 13:1570. <https://doi.org/10.3390/rs13081570>
- Hazeleger W, de Vries P, Friocourt Y (2003) Sources of the equatorial undercurrent in the Atlantic in a high-resolution ocean model. *J Phys Ocean* 33(4):677–693

34. Houndegnonto OJ, Kolodziejczyk N, Maes C, Bourlès B, Da-Allada CY, Reul N (2021) Seasonal variability of freshwater plumes in the eastern Gulf of Guinea as inferred from satellite measurements. *J Geophys Res* 126:e2020JC017041. <https://doi.org/10.1029/2020JC017041>
35. Iqbal K, Zhang M, Piao S (2020) Symmetrical and asymmetrical rectifications employed for deeper ocean extrapolations of in situ CTD data and subsequent sound speed profiles. *Symmetry* 12(9):1455. <https://doi.org/10.3390/sym12091455>
36. Jacox MG, Edwards CA (2012) Upwelling source depth in the presence of nearshore wind stress curl. *J Geophys Res* 117:C05008. <https://doi.org/10.1029/2011JC007856>
37. Jang E, Kim YJ, Im J, Park Y-G (2021) Improvement of SMAP sea surface salinity in river-dominated oceans using machine learning approaches. *GISci Remote Sens* 58(1):138–160
38. Kolodziejczyk N, Marin F, Bourlès B, Gouriou Y, Berger H (2014) Seasonal variability of the equatorial undercurrent termination and associated salinity maximum in the Gulf of Guinea. *Clim Dyn* 43:3025–3046
39. Korosov A, Counillon F, Johannessen JA (2015) Monitoring the spreading of the Amazon freshwater plume by MODIS, SMOS, Aquarius, and TOPAZ. *J Geophys Res Oceans* 120:268–283
40. Lamb PJ (1978) Case studies of tropical Atlantic surface circulation pattern during recent sub-Saharan weather anomalies, 1967–1968. *Mon Weather Rev* 106:482–491
41. Lee T, Lagerloef G, Gierach MM, Kao H-Y, Yueh S, Dohan K (2012) Aquarius reveals salinity structure of tropical instability waves. *Geophys Res Lett* 39(12):L12610-1-L12610-6
42. Maloney E, Shaman J (2008) Intraseasonal variability of the West African monsoon and Atlantic ITCZ. *J Clim* 21(12):2898–2918
43. Mears CA, Scott J, Wentz FJ, Ricciardulli L, Leidner SM, Hoffman R, Atlas R (2019) A near-real-time version of the cross-calibrated multiplatform (CCMP) ocean surface wind velocity data set. *J Geophys Res Oceans* 124:6997–7010
44. Meissner T, Wentz FJ, Manaster A, Lindsley R (2019) Remote sensing systems SMAP ocean surface salinities [level 2c, level 3 running 8-day, level 3 monthly], version 4.0 validated release. Remote Sensing Systems, Santa Rosa, CA, USA. Available online at www.remss.com/missions/smap, <https://doi.org/10.5067/SMP40-3SMCS>
45. Menezes VV (2020) Statistical Assessment of sea-surface salinity from SMAP: Arabian Sea, Bay of Bengal, and a promising Red Sea application. *Remote Sens* 12:447. <https://doi.org/10.3390/rs12030447>
46. Moon J-H, Song YT (2014) Seasonal salinity stratifications in the near-surface layer from Aquarius, Argo, and an ocean model: focusing on the tropical Atlantic/Indian oceans. *J Geophys Res Oceans* 119:6066–6077
47. Nichols RE, Subrahmanyam B (2019) Estimation of surface freshwater fluxes in the Arctic Ocean using satellite-derived salinity. *Remote Sens Earth Syst Sci* 2:247–259
48. Nyadjro ES (2021) Impacts of the 2019 Strong IOD and monsoon events on Indian Ocean Sea surface salinity. *Remote Sens Earth Syst Sci*. <https://doi.org/10.1007/s41976-021-00054-1>
49. Nyadjro ES, Rydbeck AV, Jensen TG, Richman JG, Shriver JF (2020) On the generation and salinity impacts of intraseasonal westward jets in the equatorial Indian Ocean. *J Geophys Res* 125. <https://doi.org/10.1029/2020JC016066>
50. Nyadjro ES, Subrahmanyam B (2014) SMOS satellite mission reveals the salinity structure of the Indian Ocean Dipole. *IEEE Geosci Remote Sens Lett* 11(9):1564–1568
51. Nyadjro ES, Subrahmanyam B (2016) Spatial and temporal variability of central Indian Ocean salinity fronts observed by SMOS. *Remote Sens Environ* 180:146–153
52. Rao SA, Behera SK (2005) Subsurface influence on SST in the tropical Indian Ocean: structure and interannual variability. *Dyn Atmos Oceans* 39:103–139
53. Santos-Garcia A, Jacob MM, Jones WL (2016) SMOS Near-surface salinity stratification under rainy conditions. *IEEE J Sel Top Appl Earth Obs Remote Sens* 9(6):2493–2499
54. Sommer A, Reverdin G, Kolodziejczyk N, Boutin J (2015) Sea surface salinity and temperature budgets in the North Atlantic Subtropical Gyre during SPURS experiment: August 2012–August 2013. *Front Mar Sci* 2:107. <https://doi.org/10.3389/fmars.2015.00107>
55. Song YT, Lee T, Moon J-H, Qu T, Yueh S (2015) Modeling skin-layer salinity with an extended surface–salinity layer. *J Geophys Res Oceans* 120:1079–1095
56. Sprintall J, Tomczak M (1992) Evidence of the barrier layer in the surface layer of the tropics. *J Geophys Res* 97:7305–7316
57. Tang W, Fore A, Yueh S, Lee T, Hayashi A, Sanchez-Franks A et al (2017) Validating SMAP SSS with in situ measurements. *Remote Sens Environ* 200:326–340. <https://doi.org/10.1016/j.rse.2017.08.021>
58. Tzortzi E, Josey S, Srokosz M (2013) Tropical Atlantic salinity variability: new insights from SMOS. *Geophys Res Lett* 40(10):2143–2147
59. Vinogradova N, Lee T, Boutin J, Drushka K, Fournier S, Sabia R, Stammer D, Bayler E, Reul N, Gordon A et al (2019) Satellite salinity observing system: recent discoveries and the way forward. *Front Mar Sci* 6:243
60. Wiafe G, Nyadjro ES (2015) Satellite observations of upwelling in the Gulf of Guinea. *IEEE Geosci Remote Sens Lett* 12(2):1066–1070. <https://doi.org/10.1109/LGRS.2014.2379474>

Publisher's Note Springer Nature remains neutral with regard to jurisdictional claims in published maps and institutional affiliations.